Supporting Information

Nanoclay modulated copper cysteamine composites for enhanced fluorescence

Qianqian Liu,[a] Hao Wang,[bcd] Xiaozheng Liang,[a] Yili Tang,[e] and Huaming Yang[abcd]*

[a] *Hunan Key Laboratory of Mineral Materials and Application, School of Minerals Processing and Bioengineering, Central South University, Changsha 410083, China.*

[b] *Engineering Research Center of Nano-Geomaterials of Ministry of Education, China University of Geosciences, Wuhan 430074, China.*

[c] *Laboratory of Advanced Mineral Materials, China University of Geosciences, Wuhan 430074, China.*

[d] *Faculty of Materials Science and Chemistry, China University of Geosciences, Wuhan 430074, China.*

[e] *School of Chemistry and Chemical Engineering, Central South University, Changsha 410083, China.*

* Corresponding author: hmyang@csu.edu.cn, hm.yang@cug.edu.cn (H. Yang)

Table of contents

Experimental section

Materials

All chemical reagents were purchased from Shanghai Aladdin Biochemical Technology Co., Ltd. (China), namely, montmorillonite (MMT), sodium hydroxide (NaOH), Copper (II) chloride dihydrate ($CuCl_2 \cdot 2H_2O$), 2-mercaptoethylamine hydrochloride. All chemical substances used in our work were analytical grade. The reaction solvent was used deionized (DI) water without further purification.

Synthesis of CC and MCC

Copper cysteamine (CC) and montmorillonite-copper cysteamine composite (MCC) were synthesized referring to the published method.[1] Different amounts of MMT after ball milling was dispersed in 200 mL water and sonicated for 30 min. Next, by stirring, 0.728 g $CuCl_2 \cdot 2H_2O$ and 1.016 g cysteamine were taken into the MMT solution and uniform distribution. Then, the pH value was corrected to 7.12 by adding 1 M NaOH solution. The uniform solution was future stirred at room temperature for 2 h. Then, the uniform solution was transferred to an oil bath and kept at 100 °C for 30 min. Next, the suspension was centrifuged at 10000 rpm for 5 min and washed with a solution of DI water and ethanol (v/v = 5:4) to remove impurities. Eventually, the particles were freeze-dried. MMT was added at 0, 50, 150, 300, and 450 mg during the synthesis process.

Characterization

The samples were characterized to investigate the structural characterizing by X-ray diffraction (XRD) and were recorded at the D8 ADVANCE (Bruker, Germany) using Cu Kα radiation (λ = 0.154 nm) with 2θ scanning from 5 to 90°, 5° min^{-1} in the continuous mode. X-ray photoelectron spectroscopy (XPS) test was using a Thermo Scientific K-Alpha (Thermo, USA). The peak position of C1s in the sample was adjusted at 284.8 eV. The metal ion content was evaluated by an inductively coupled plasma optical emission spectroscopy (ICP-OES, Thermo Fisher iCAP PRO, Thermo, USA). The microstructural configuration was investigated using transmission electron microscopic (TEM, Thermo Fisher Talos F200s, Thermo, USA) and scanning electron microscope (SEM, ZEISS Gemini 300, Germany). Fourier transform infrared spectrometer (FTIR) was measured using a Nicolet iS50 spectrograph (Thermo, USA). The NanoBrook 90plus PALS (Bruker, USA) appraised the zeta potential of samples. The UV-Visible/NIR spectra of samples were detected using the UH4150 spectrophotometer (Hitachi, Japan). The photoluminescence excitation (PLE) and photoluminescence emission (PL) spectra

of samples were measured by a fluorescence spectrophotometer (F-4700, Hitachi, Japan). The time-resolved photoluminescence spectra and absolute quantum yield are estimated using the Edinburgh FLS1000 spectrometer (UK). The decay curve fitted a double exponential decay equation (1).[1]

$$I = I_1 exp\left(-\frac{t}{\tau_1}\right) + I_2 exp\left(-\frac{t}{\tau_2}\right) \quad (1)$$

The radiative (k_r) and nonradiative decay rate (k_{nr}) constant of the material was calculated by equations (2),[2] (3), and (4).[1]

$$\tau^{-1} = k_r + k_{nr} \quad (2)$$

$$k_r = \frac{\Phi}{\tau} \quad (3)$$

$$k_{nr} = \frac{1 - \Phi}{\tau} \quad (4)$$

Computational Methods

All theoretical calculations were carried out using the first-principles to carry out all spin-polarization density functional theory (DFT) calculations and within the generalized gradient approximation (GGA) utilizing the Perdew-Burke-Ernzerhof (PBE) formulation.[3-5] The ionic cores were represented in the projected augmented wave (PAW) potentials,[6,7] and valence electrons into account through a plane wave basis put with a kinetic energy cutoff of 450 eV. Partial occupancies of the Kohn-Sham orbitals were chosen using the Gaussian smearing method and a width of 0.05 eV. The energy change was smaller than 10^{-5} eV suggesting the electronic energy was considered self-consistent. The energy change was smaller than 0.02 eV $Å^{-1}$ means a geometry optimization was considered convergent. The 18 Å vacuum layer was joined to the surface to eliminate the artificial interactions between periodic images. The weak interaction was described through the DFT+D3 method utilized empirical correction in Grimme's scheme.[8,9] The adsorption energy can be calculated by equation (5).

$$E_{ads} = E_{MCC} - (E_{MMT} + E_{CC}) \quad (5)$$

Preparation of Luminescent Ink

The 6% polyvinylidene alcohol (PVA) solution was stirred at 90 °C until a transparent solution was formed. Subsequently, MMT, CC, and MCC powder were added and ultrasonically mixed. The mixed solution was stirred and heated to disperse the materials more evenly. The thoroughly blending solution was printed on the non-fluorescent filter paper and dried at 60 °C for 2 h. Finally, the pictures under 365 nm ultraviolet (UV) light irradiation were acquired using

a digital camera (D3200, Nikon, Japan).

Antibacterial Performance of CC and MCC

The agar diffusion test and optical density (OD) value test at 600 nm were used to observe the antibacterial activity of MMT, CC, and MCC. The gram-positive bacteria *Staphylococcus aureus* (*S. aureus*, ATCC 25923) was selected for the experiment. First, the bacteria were cultured in 5 mL of fresh Luria-Bertani (LB) medium for 4 h at 37 °C stable temperature environment. Then, the bacterial solution was diluted, and added 96-well culture plate was incubated with MMT, CC, and MCC at 37 °C for 12 h. Next, the solution was collected OD600 using a multimode microplate reader (Spark, Tecan, Switzerland). In addition, the solution was diluted for plate coating. Observe after incubation overnight. For the agar diffusion test, the filter paper was soaked in different PVA materials and dried at 60 °C for 2 h. It was then perforated with a hole punch. The circular filter paper was placed in the center of the agar plate. The bacterial suspension was added, grown on the agar plate, and then incubated at 37 °C for 24 h. The inhibition zone reflected the results.

Measurement of ROS

This study used 2, 7-dichlorodihydrofluorescein (DCFH) as the fluorescent probe. The deacetylation of 2',7'-Dichlorodihydrofluorescein diacetate (DCFH-DA) was chemically hydrolyzed to DCFH by adding a strong base of NaOH. The solution was reacted in the dark at room temperature for 30 min. The working solution was prepared by dilution with PBS. Then, add 0.1 mL of MMT, CC, and MCC solution to 1.9 mL of DCFH solution with and without 365 nm UV treatment. The fluorescence generated by the DCFH oxidation was measured continuously at 485 nm excitation and 530 nm emission.

In *Vitro* Hemolytic Assay

Fresh anticoagulant rabbit blood was washed with PBS and prepared into a 5% red blood cell suspension. 500 μL material solution and 500 μL erythrocyte suspension were added in different tubes. These hybrid solutions were incubated at 37 °C for 1 h. PBS (pH 7.4) and H_2O were negative and positive reaction controls. Subsequently, the reaction was stopped by centrifugation. The supernatant was detected with a multimode microplate reader for OD545. The hemolytic index (%) was measured mathematically by the following formulae equation (6).

$$Hemolytic\ index\ = \frac{OD_{Sample} - OD_{Negative\ Control}}{OD_{Positive\ Control} - OD_{Negative\ Control}} \times 100\% \qquad (6)$$

Statistical Analysis

All experimental results were statistically represented as mean ± standard deviations. SPSS 19.0 was used to analyze the difference between specimens. The normality of the variables was evaluated using a one-way analysis of variance (ANOVA) following Dunnet's two-sided *t*-test.

Supplementary Results

Fluorescence intensity analysis

MCC was synthesized by adding 0, 50, 150, 300, and 450 mg of MMT, respectively. Fig. S3a shows the PLE spectra of all samples under 607 nm-wavelength emission. The excitation wavelength signal was detected in the range of 320–400 nm region. Sample 0 mg has the lowest peak. Fig. S3b shows the PL spectra of all samples exposed to 365 nm-wavelength excitations. An emission of orange light, at 607 nm, was observed. Sample 0 mg has the lowest peak. The above results indicate that the addition of MMT can enhance the fluorescence intensity of CC.

Antimicrobial effect and antimicrobial mechanism analysis

The antibacterial effectiveness of CC and that of the MCC composite were tested using *S. aureus* (Fig. S6, ESI†). The results show that the survival rate of CC and MCC was 6.22%. and 21.54%. After UV irradiation, the survival rate of CC and MCC was 7.15% and 13.58%. This experimental result was also verified by counting the number of colony-forming units on LB agar plates. One of the characteristics of CC is that it can generate reactive oxygen species (ROSs) to kill bacteria.[1,10] Therefore, the production of ROSs was examined. As shown in Fig. S7 (ESI†). the generation of ROS by CC was enhanced under UV light irradiation. The results showed that MCC also produced ROSs and displayed bactericidal activity. In addition, the changes in the surface membrane structures of *S. aureus* were examined by TEM following the coculture with CC and MCC. Compared with untreated *S. aureus,* the shape of the bacteria coculture with CC and MCC changed significantly. The cell surface was seriously ruptured, and the cell contents leaked (Fig. S8, ESI†).

Hemolysis analysis

To test the safety of each material, we conducted a hemolysis test. The hemolysis percentages of MMT, CC, and MCC were 78.28%, 6.12%, and 3.95%, respectively. The hemolysis percentage of MCC was lower than the criterion defined by ASTM F756-08. The lower the hemolysis, the higher the safety.[11-13] Thus, of the three materials tested, MCC was concluded to display the best compatibility with blood (Fig. S9, ESI†).

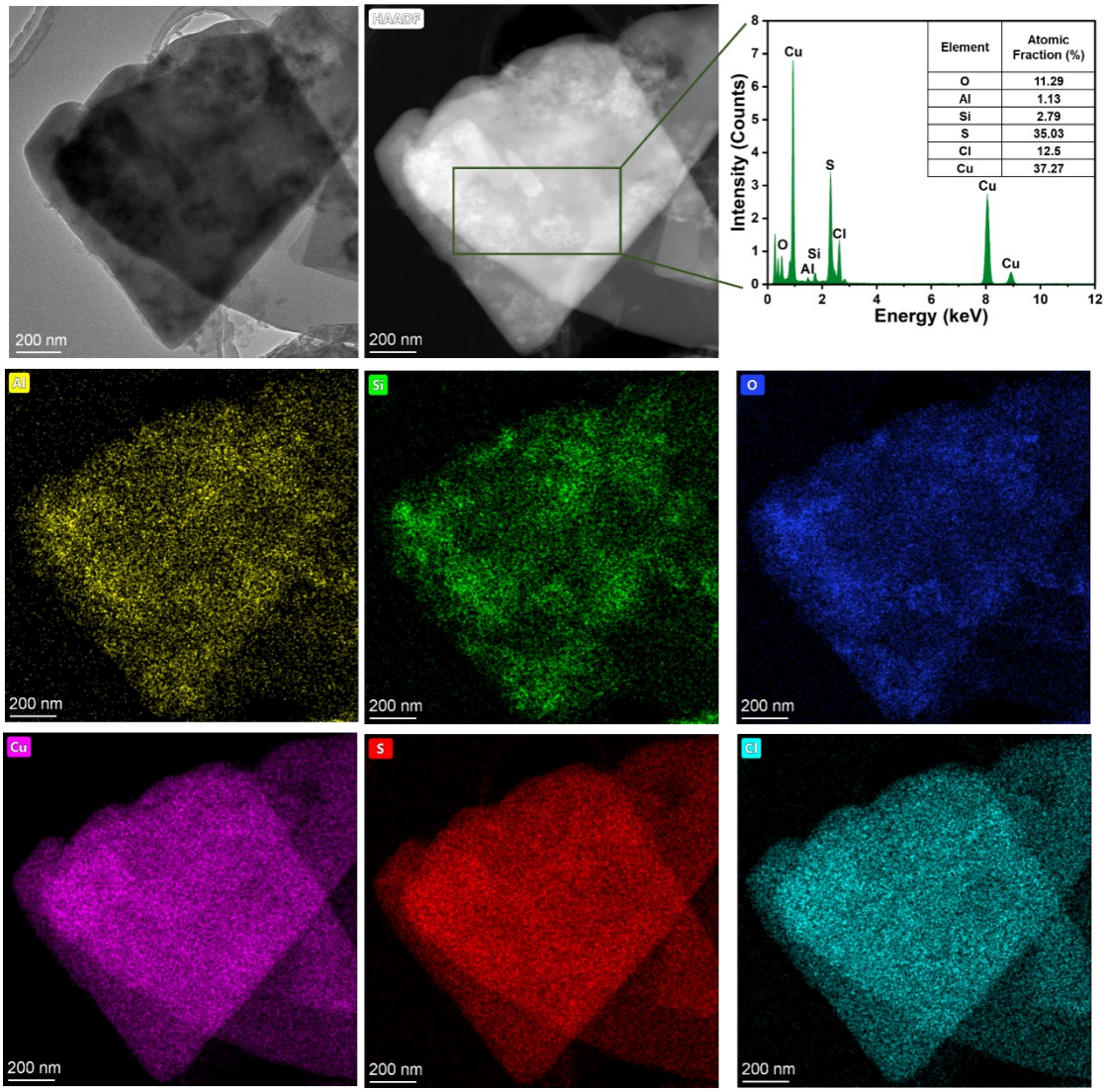

Fig. S1. TEM image, EDX spectrum, and mapping images of MCC.

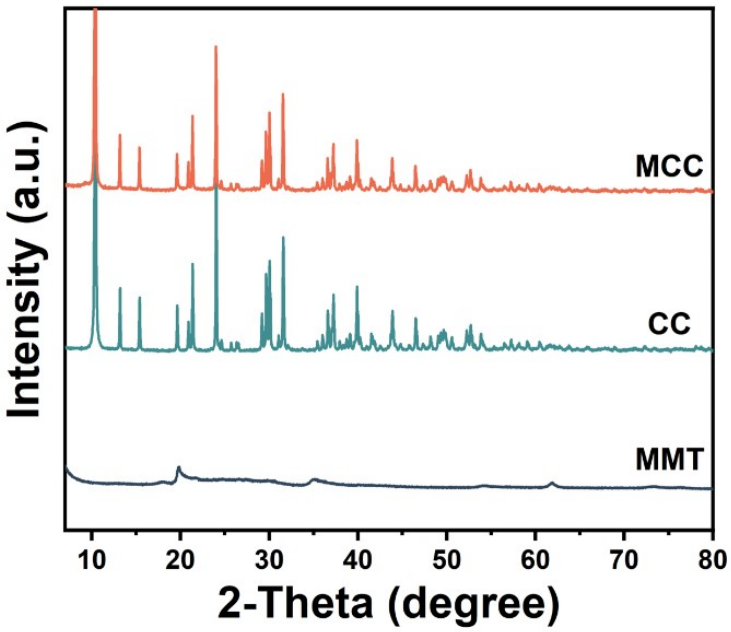

Fig. S2. XRD patterns of MMT, CC, and MCC.

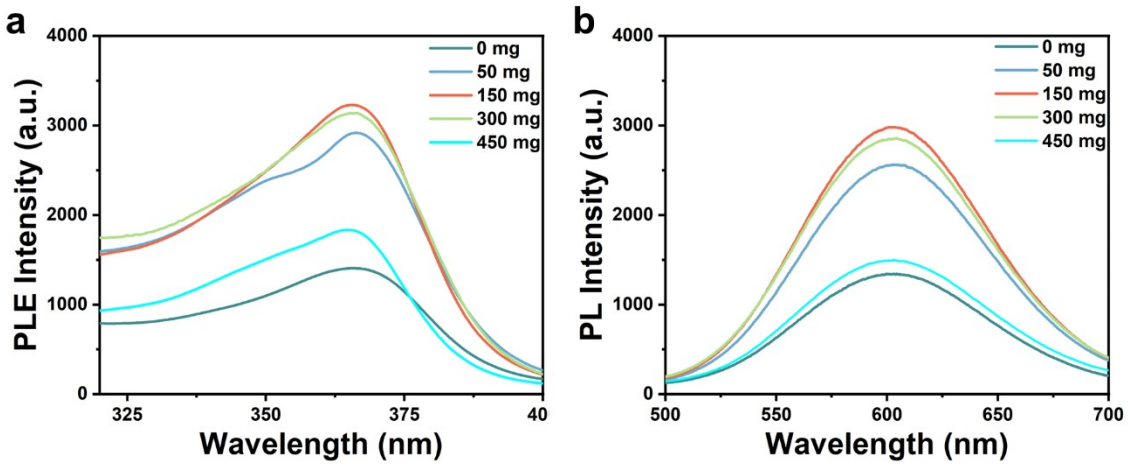

Fig. S3. Comparison of (a) PLE spectra at 607 nm and (b) PL spectra at 365 nm of CC and MCC powders with 0 mg, 50 mg, 150 mg, 300 mg, and 450 mg of MMT during synthesis.

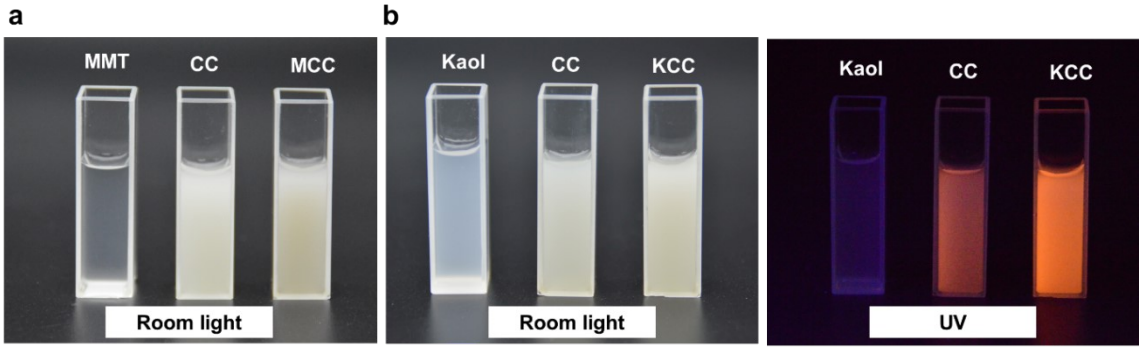

Fig. S4. (a) MMT, CC, and MCC particles suspended in water under room light. (b) Kaol, CC, and KCC particles were suspended in water under room light and UV light (365 nm).

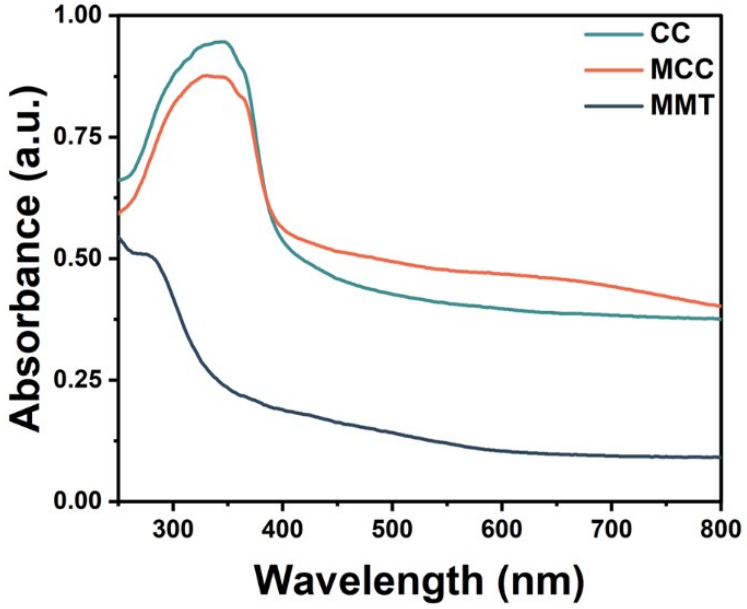

Fig. S5. Comparison of UV-visible absorption spectra of MMT, CC, and MCC powders.

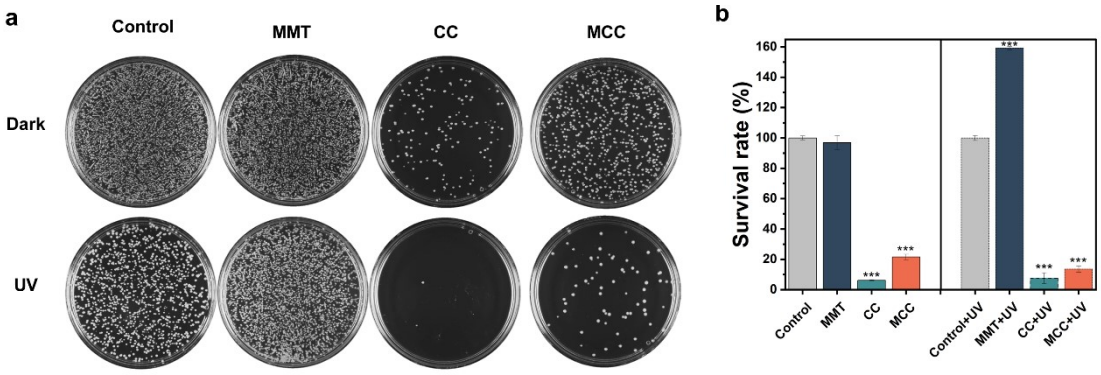

Fig. S6. (a) Photographs of colonies and (b) quantitative analysis of *S. aureus* in MMT, CC, and MCC groups treated with or without 365 nm UV exposure for 10 min. Values are means ± SD. *$p < 0.05$, **$p < 0.01$and ***$p < 0.001$ vs control group.

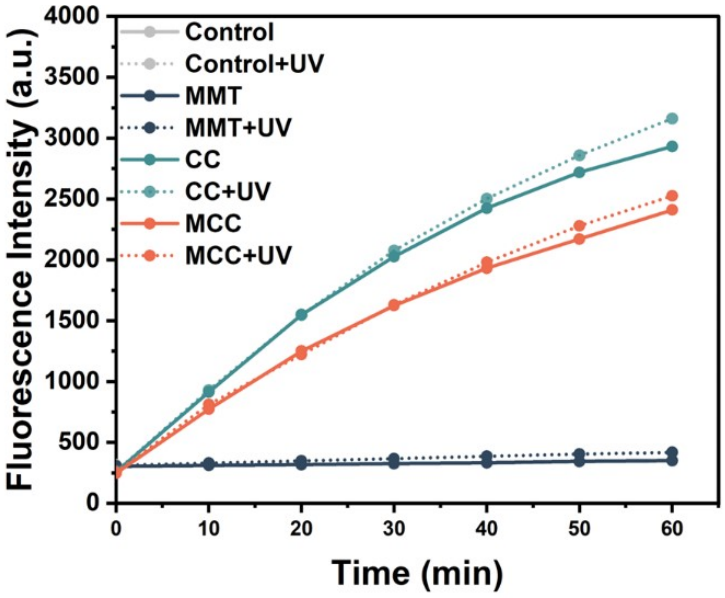

Fig. S7. The ROS production in MMT, CC, and MCC under UV light (365 nm) and room light.

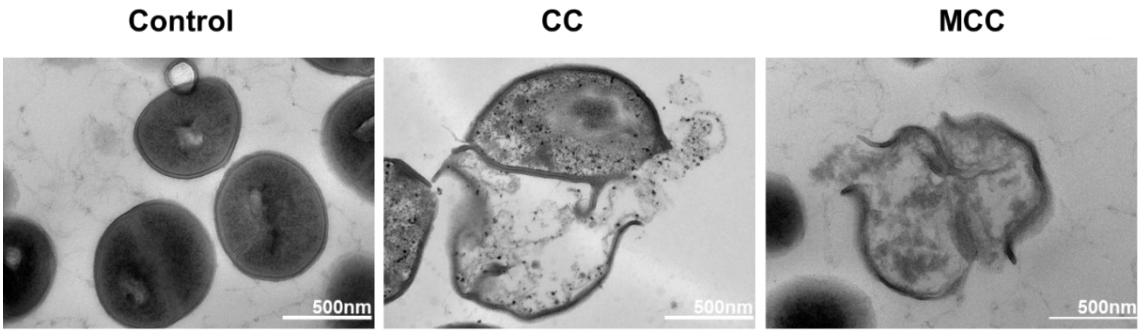

Fig. S8. TEM images of *S.aureus* treated with CC, and MCC.

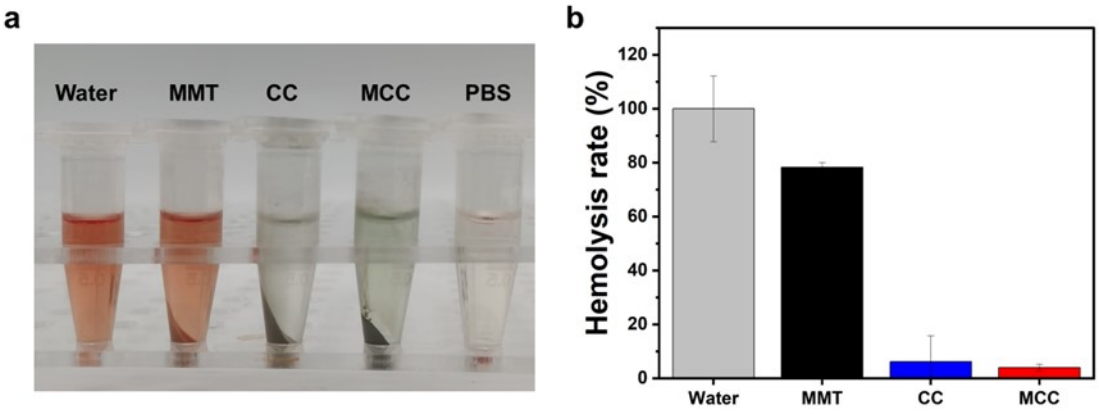

Fig. S9. (a) Hemolysis image and (b) hemolysis rates of MMT, CC, and MCC.

Table S1 DFT distances (Å) and bond angles (°) of CC and MCC

	CC	MCC
Cu(1)-S(1)*	2.21	2.24
Cu(1)-Cl	2.27	2.27
Cu(1)-S(1)	2.21	2.27
Cu(2)-S(1)	2.29	2.20
Cu(2)-N	2.07	2.09
Cu(2)-S(2)	2.56	2.29
S(2)-Cu(2)-N	85.12	90.49
N-Cu(2)-S(1)	107.07	116.94
S(2)-Cu(2)-S(1)	112.52	150.56
Cu(2)-S(1)-Cu(1)	94.45	105.73
S(1)-Cu(1)-S(1)*	119.04	129.22
S(1)-Cu(1)-Cl	120.48	120.56

Table S2 Photophysical properties

Compound	$\lambda_{abs.max}$ (nm)	$\lambda_{em.max}$ (nm)	τ_1/μs	τ_2/μs	τ/μs	Φ	[a] $k_r/10^4 s^{-1}$	[b] $k_{nr}/10^4 s^{-1}$
CC	365	607	2.62	13.98	6.58	0.59%	0.09	15.11
MCC	365	607	4.43	15.41	8.36	1.16%	0.14	11.82

[a] $k_r=\Phi/\tau$

[b] $k_{nr}=(1-\Phi)/\tau$

References

1. L. Ma, W. Chen, G. Schatte, W. Wang, A. G. Joly, Y. Huang, R. Sammynaiken and M. Hossu, *J. Mater. Chem. C.*, 2014, **2**, 4239-4246.
2. R. Hamze, J. L. Peltier, D. Sylvinson, M. Jung, J. Cardenas, R. Haiges, M. Soleilhavoup, R. Jazzar, P. I. Djurovich, G. Bertrand and M. E. Thompson, *Science*, 2019, **363**, 601-606.
3. G. Kresse and J. Furthmüller, *Comp. Mater. Sci.*, 1996, **6**, 15-50.
4. G. Kresse and J. Furthmüller, *Phys. Rev. B*, 1996, **54**, 11169-11186.
5. J. P. Perdew, K. Burke and M. Ernzerhof, *Phys. Rev. Lett.*, 1996, **77**, 3865-3868.
6. P. E. Blöchl, *Phys. Rev. B*, 1994, **50**, 17953-17979.
7. G. Kresse and D. Joubert, *Phys. Rev. B*, 1999, **59**, 1758-1775.
8. S. Grimme, J. Antony, S. Ehrlich and H. Krieg, *J. Chem. Phys.*, 2010, **132**, 154104.
9. S. Grimme, S. Ehrlich and L. Goerigk, *J. Comput. Chem.*, 2011, **32**, 1456-1465.
10. Q. Zhang, X. Guo, Y. Cheng, L. Chudal, N. K. Pandey, J. Zhang, L. Ma, Q. Xi, G. Yang, Y. Chen, X. Ran, C. Wang, J. Zhao, Y. Li, L. Liu, Z. Yao, W. Chen, Y. Ran and R. Zhang, *Signal Transduction Targeted Ther.*, 2020, **5**, 58.
11. A. Roy, M. Joshi, B. S. Butola and S. Malhotra, *Mater. Sci. Eng., C*, 2018, **93**, 704-715.
12. X. Tong, Z. Shi, L. Xu, J. Lin, D. Zhang, K. Wang, Y. Li and C. Wen, *Acta Biomater.*, 2020, **102**, 481-492.
13. R. Yue, J. Niu, Y. Li, G. Ke, H. Huang, J. Pei, W. Ding and G. Yuan, *Mater. Sci. Eng., C*, 2020, **113**, 111007.